nature materials

ARTICLES

PUBLISHED ONLINE: 13 APRIL 2014 | DOI: 10.1038/NMAT3938

Universal process-inert encoding architecture for polymer microparticles

Jiseok Lee[1†], Paul W. Bisso[1,2†], Rathi L. Srinivas[1], Jae Jung Kim[1], Albert J. Swiston[2] and Patrick S. Doyle[1*]

Polymer microparticles with unique, decodable identities are versatile information carriers with a small footprint. Widespread incorporation into industrial processes, however, is limited by a trade-off between encoding density, scalability and decoding robustness in diverse physicochemical environments. Here, we report an encoding strategy that combines spatial patterning with rare-earth upconversion nanocrystals, single-wavelength near-infrared excitation and portable CCD (charge-coupled device)-based decoding to distinguish particles synthesized by means of flow lithography. This architecture exhibits large, exponentially scalable encoding capacities ($>10^6$ particles), an ultralow decoding false-alarm rate ($<10^{-9}$), the ability to manipulate particles by applying magnetic fields, and pronounced insensitivity to both particle chemistry and harsh processing conditions. We demonstrate quantitative agreement between observed and predicted decoding for a range of practical applications with orthogonal requirements, including covert multiparticle barcoding of pharmaceutical packaging (refractive-index matching), multiplexed microRNA detection (biocompatibility) and embedded labelling of high-temperature-cast objects (temperature resistance).

Encoded microparticles are attractive as information carriers owing to their small size and ability to serve as scaffolds for functional payloads such as molecular sensors[1–19]. However, satisfying the exacting specifications of industrial functions such as anti-counterfeiting, massively parallelized bioassays, or forensic labelling has proved elusive. Unique encoding of single units within information-intensive processes such as pharmaceutical packaging entails encoding capacities of 10^5–10^{12} and high-throughput particle synthesis, which is out of reach for many present systems[1–3,5–17]. Exposure to harsh environments requires thermal insensitivity, biocompatibility and/or chemical resistance. Furthermore, simple, portable decoding equipment avoids crippling implementation complexity, yet must retain the capability for low-error readout in the presence of confounding factors (for example, complex background, obscurants or noise). Present encoding architecture designs focus on advancing the capabilities of individual components—encoding, synthesis, or decoding methodologies—at the expense of overall performance[3–18,20]. For instance, innovative graphical encoding architectures in which codes are represented by a binary two-dimensional pattern have achieved some commercial success, but are intrinsically limited to encoding capacities $<10^3$ (ref. 10) and cannot be robustly decoded with a portable device[3,4]. Purely spectral approaches are limited by the need for precise loading of multiple dyes[13–17], challenging spectral deconvolution[11–18], or cumbersome and expensive decoding equipment[13,16,18]. A recent hybrid spectral/graphical approach combined magnetic inks (M-Ink) and flow lithography, yet is severely constrained by synthesis throughput and code reproducibility[4]. Another innovative hybrid spectral/graphical approach uses combinatorial attachment of fluorescent reporter beads to a support bead, but requires sophisticated flow cytometry, confocal microscopy and image deconvolution for accurate readout[20]. Most architectures are also narrowly designed for use in multiplexed bioassays, artificially limiting the accessible application space[1–18,20].

As a solution, we employ a rational multiscale design strategy to engineer a robust encoding method for compatibility with high-throughput particle synthesis and portable CCD-based decoding. The resulting architecture exhibits pronounced insensitivity to particle chemistry—enabling tuning of encoding capacity and decoding error rate independently of particle material properties—as well as the capacity for straightforward magnetic manipulation. We demonstrate quantitatively predictable decoding of both temperature-resistant and biocompatible particles in challenging, realistic environments. With single-particle encoding capacities in excess of 1 million and error rates of less than 1 part per billion (ppb), we expand the practically accessible number of codes for applications such as forensic product labelling and multiplexed bioassays by orders of magnitude[1,2]. Extending the use of encoded particles to a broad and evolving range of previously unexplored industrial applications, we also introduce a new procedure to produce covert, durable anti-counterfeiting labels with practically unlimited encoding capacity from small sets of uniquely encoded particles.

Microparticle synthesis and encoding motif

We generate unique particle barcodes by micropatterning spectrally distinct upconversion nanocrystals (UCNs). This intuitive coding motif scales exponentially as C^S for asymmetric particles (Supplementary Fig. 14) and $C^S/2$ for symmetric particles (Fig. 1c), where C is the number of distinguishable spectral signatures (UCN 'colours') and S is the number of spatial features (microparticle 'stripes'). Thus, a modest number of colours may be coupled with a similarly modest number of stripes to yield considerable encoding capacities that scale rapidly with incremental changes to either quantity. To implement this approach,

[1]Department of Chemical Engineering, Massachusetts Institute of Technology, Cambridge, Massachusetts 02139, USA, [2]Massachusetts Institute of Technology Lincoln Laboratory, Lexington, Massachusetts 02420, USA. †These authors contributed equally to this work. *e-mail: pdoyle@mit.edu

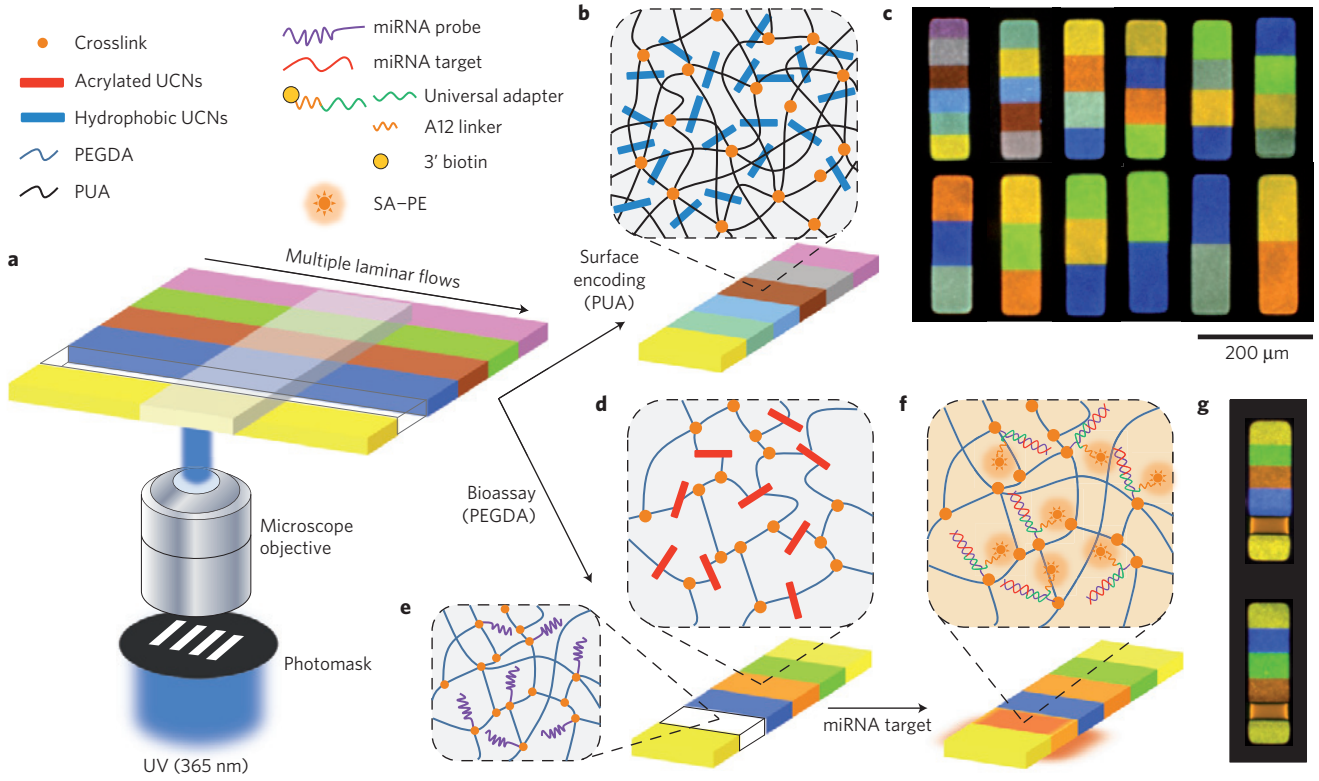

Figure 1 | Synthesis of encoded particles by stop-flow lithography. a, Multiple co-flows of monomer solution (PEGDA or PUA) with UCNs were photopolymerized in a PDMS channel through illumination with photomask-patterned ultraviolet light (365 nm) and collected for future use. **b**, Hydrophobic UCNs are physically entrained in the tightly crosslinked PUA matrix. **c**, Luminescence images of encoded PUA particles. **d**, Acrylated UCNs covalently incorporated into the mesoporous PEGDA matrix. **e**, Incorporation of acrylated miRNA probes during flow lithography for bioassay application. The mesoporous matrix allows diffusion of large (>10 nm) biomolecules through the matrix. **f**, Labelling of hydrogel particles after incubation with miRNA targets using a biotinylated universal adapter sequence and streptavidin–phycoerythrin (SA–PE). **g**, Luminescence images of encoded PEGDA hydrogel particles after miRNA bioassay (excitation, 1 W 980 nm NIR diode laser).

we use a versatile, high-performance stop-flow lithography (SFL) technique for synthesizing chemically anisotropic particles[3,21,22]. In a semicontinuous process, multiple co-flowing laminar streams—each containing a single optically active UCN moiety or probe molecule—are convected into a microchannel formed from either poly(dimethylsiloxane) PDMS or a non-swelling thiolene-based resin for use with organic solvents[23], stopped, and photopolymerized in place using mask-patterned ultraviolet light (365 nm) to form barcoded particles at a rate of 18,000 particles h^{-1}, which are then displaced when flow resumes (Fig. 1a). This $\sim 10^4$ particles h^{-1} synthesis rate is by no means limiting; hydrodynamic flow focusing has been used to increase the synthesis rate for similar particles to over 10^5 particles h^{-1} (ref. 24). The synthesis platform may also be constructed using commercial off-the-shelf parts and free-standing optics for under US$3,000, a price that includes a high-performance CCD detector (Supplementary Fig. 13). Parallelization in an industrial setting, with no further optimization, could readily increase the facility-scale synthesis throughput by orders of magnitude to meet industrial demand. Although this spatial–spectral motif is described in recent literature, other implementations use exotic materials or synthesis set-ups that do not permit scalable parallelization, giving rise to challenging processing requirements, restricted synthesis throughput and poor decoding robustness[4,5,7–10].

Embedding and spectral tuning of rare-earth UCNs

Rare-earth UCNs, an emerging class of bright anti-Stokes emitters with tunable spectral properties, enable our architecture to thrive in non-ideal industrial settings[25–30]. Individual UCNs absorb continuous-wave near-infrared (NIR) light at a single wavelength and emit in multiple narrow bands of the visible spectrum[27,28]. Large anti-Stokes shifts reduce spectral interference from sample autofluorescence and lead to enhanced decoding signal-to-noise ratios[25–28]. In contrast to M-Ink or quantum dots, these benefits persist even in the presence of obscurants or a complex, reflective background (Supplementary Movie 1). Tuning of emission intensities in multiple bands by adjusting relative stoichiometries of lanthanide dopants permits ratiometrically unique spectral encoding, in which the ratio of integrated intensities in 2 or more bands serves as the code, rather than absolute intensity[28,30]. External standards (as with porous silicon crystals), precise dye loading (as with quantum dots and Luminex), sensitive instrumentation (as with M-Ink) and extensive calibration thus become unnecessary for precision readout, paving the way for unsophisticated CCD-based decoding tools[4,12–17,19].

Figure 1 illustrates integration of UCNs into physicochemically distinct microparticles by rationally specifying UCN nanostructure and surface chemistry. We explored two different particle monomer chemistries—hydrophobic poly(urethane) acrylate (PUA; Fig. 1b,c) for thermal- and chemical-resistant microparticles and hydrophilic poly(ethylene glycol) diacrylate (PEGDA; Fig. 1d–g) for biocompatible and mesoporous microparticles that allow diffusion of large biological macromolecules[31]. For the more densely crosslinked PUA particles, we reasoned that hydrophobic UCN surface chemistry and large, rod-like UCN nanostructure would enable homogeneous and irreversible physical entrainment[32]. Integration with PEGDA particles, in contrast, requires hydrophilic surface chemistry with an ultraviolet-active functional group for

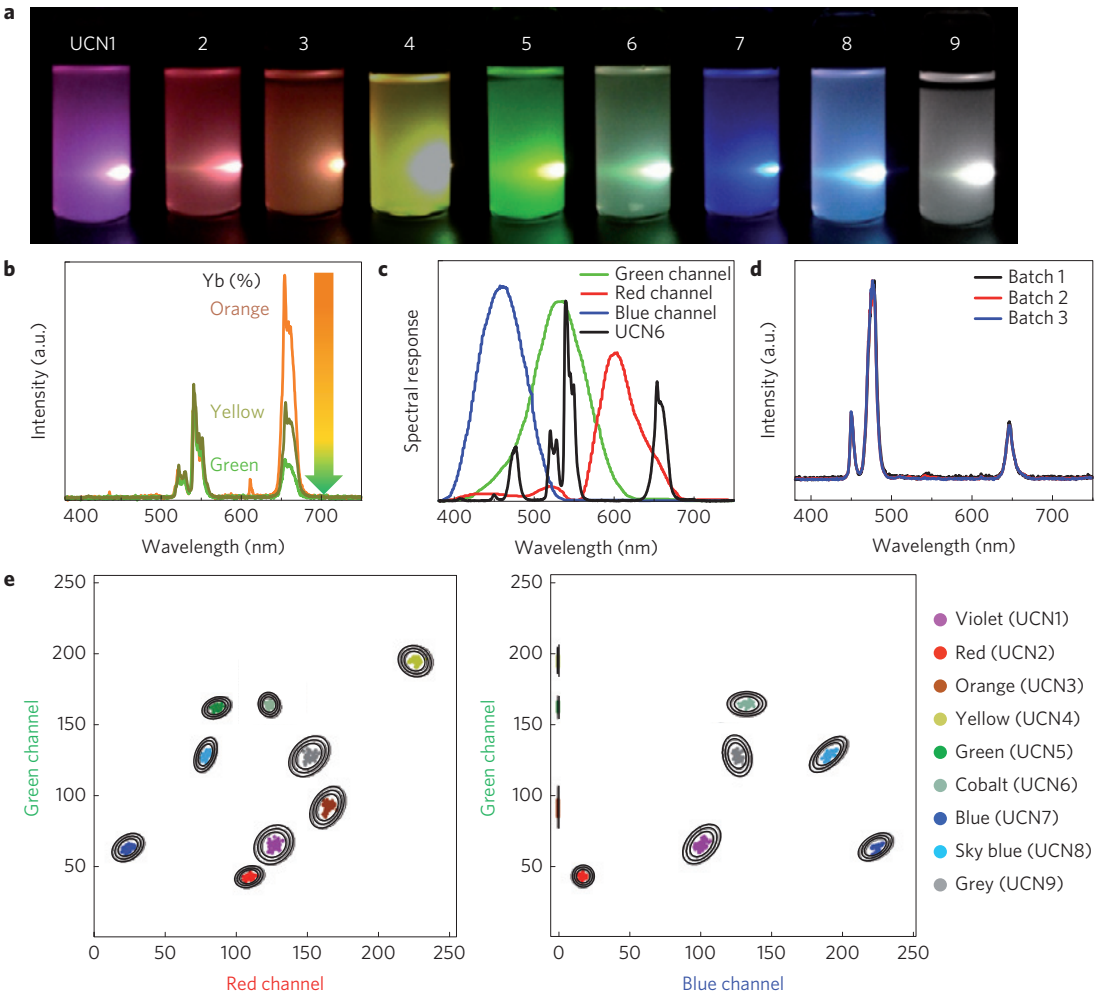

Figure 2 | Spectral characterization of UCNs. a, Luminescence images of UCN1-9 suspensions in cyclohexane on 980 nm NIR excitation. **b**, Ratiometrically unique upconversion emission spectra produced by varying dopant concentrations. **c**, Overlay of UCN emission spectrum with CCD spectral response (Nikon D200) for output RGB prediction. **d**, Overlay of normalized emission spectra for 3 batches of UCN7. **e**, RGB scatter plots for encoded particles indicating particle-to-particle spectral reproducibility. Ellipses around each colour cluster represent 3-, 4- and 5-sigma contours obtained by fitting a Gaussian mixture model ($n = 50$).

strong, covalent incorporation. We synthesized long (>250 nm in length), high-aspect-ratio UCNs coated in oleic acid through a scalable batch hydrothermal route[25] (Supplementary Figs 1 and 2; see Methods for details). These UCNs are readily dispersed in a blend of PUA monomer and photo-initiator for use in SFL synthesis. Hydrophilic UCNs were formed by sequential oxidation and partial acrylation of the oleic acid ligands, enabling excellent dispersion in PEGDA premixes while permitting ultraviolet-mediated crosslinking to inhibit leaching[29] (Supplementary Fig. 3; see Supplementary Information for surface chemistry modification protocol details). Images taken under 1 W 980 nm continuous-wave laser illumination demonstrate successful incorporation of UCNs into SFL-synthesized microparticles with markedly different physicochemical properties (Fig. 1c (PUA) and 1g (PEGDA)).

We synthesized a palette of 9 spectrally distinct UCNs by adjusting the relative stoichiometries of the lanthanide ions Yb^{3+}, Er^{3+} and Tm^{3+} in the UCN reaction premix, resulting in narrow emission bands centred at 470 (blue), 550 (green) and 650 nm (red) (Fig. 2a; refs 28,30). Importantly, lanthanide dopant stoichiometries have little bearing on UCN nanostructure and surface chemistry[25–28], decoupling control of the encoding method from particle chemistry, and hence, material properties. Increasing Yb^{3+} doping in the presence of light Er^{3+} co-doping led to consistent increases in red/green intensity ratios (Fig. 2b). Decreasing the Er/Tm ratio in Yb–Er–Tm co-doped UCNs led to increases in blue/green intensity ratios (dopant concentrations summarized in Supplementary Table 1). The result of this strategy is an initial set of 9 bright, ratiometrically unique UCNs, excited at the same NIR wavelength, that may be distinguished readily by the naked eye (Fig. 2a). By embedding different UCNs within barcoded microparticles consisting of up to 6 stripes, an encoding capacity of greater than 1 million is easily achieved (Fig. 1c,g and Supplementary Fig. 14). To augment encoding capacity, the palette of spectrally distinct UCNs may be further expanded by adjusting Yb/Er/Tm ratios with negligible impact on the decoding error rate. Moreover, particles with an additional stripe would boost encoding capacities to over 10 million, while requiring little more than an additional input port on the microfluidic synthesis device.

Characterization of UCN-encoded microparticles

Spectral reproducibility is the critical link between large, scalable encoding capacities and exceptional decoding robustness. In suspension, we observed pronounced insensitivity of UCN upconversion emission spectra to batch-to-batch synthesis variations (Fig. 2d, $n = 3$), surface chemistries and chemical environments (Supplementary Fig. 7). We synthesized barcoded

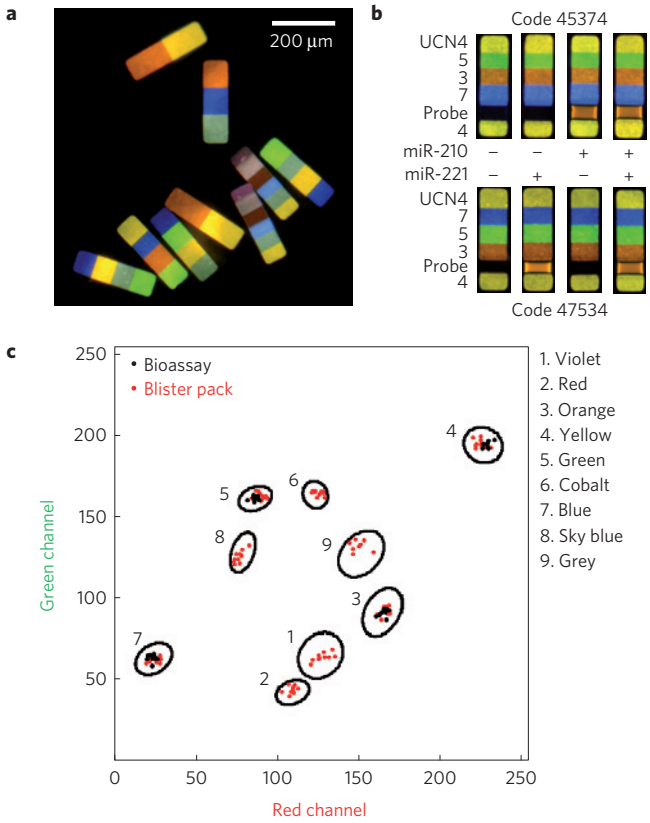

Figure 3 | CCD-based decoding of encoded particles. a,**b**, Luminescence images of encoded PUA particles on a pharmaceutical blister pack (**a**) and a multiplexed miRNA bioassay (**b**). **c**, Code-calling using red–green (RG) scatter plots for multiplexed bioassay (black) and multi-particle encoding of pharmaceutical blister pack (red). Ellipses represent 5-sigma contours obtained from separate training data (excitation, 1 W 980 nm NIR diode laser; CCD, Nikon D200).

PEGDA (UCNs 3–5 and 7) and PUA (UCNs 1, 2, 6, 8 and 9) particles and acquired images with a digital camera and microscope objective under NIR illumination (Methods for details). We fit scatter plots of R versus G and G versus B values for individual stripes to a Gaussian mixture model (Fig. 2e), and observed an average coefficient of variation of 2% (Supplementary Table 2). This corresponds to an average standard deviation of 2.1 RGB units (on a scale of 255) for separately acquired images of separately synthesized particles, indicating outstanding particle-to-particle reproducibility. In addition, error ellipses are non-overlapping to better than 6 sigma, indicating that decoding error rates of less than 1 ppb are to be expected (Fig. 2e). Multiple independent rounds of SFL synthesis exhibit excellent particle uniformity (Supplementary Fig. 9 and Table 4). Particles are immune to photobleaching[11]; no change in emission intensity was observed over 20 minutes of continuous NIR excitation at 10^3 W cm^{-2} (Supplementary Fig. 6), and emission intensity was constant over the course of at least a month (Supplementary Fig. 3). Strikingly, when we convolved the upconversion emission spectrum of UCNs in solution with the spectral response curves of our Nikon D200 camera, RGB values predicted from convolution tightly matched the centroids of those measured experimentally, independent of particle chemistry (Supplementary Fig. 5 and Table 3). The ability to broadly predict decoding results from UCN spectra provides a framework for rapid, confident code set generation, conferring significant advantages over other architectures' laborious and lengthy design processes[4–8,10–19].

Demonstration of surface encoding

To demonstrate this architecture's extraordinary flexibility and practical utility, we introduce a new, covert labelling method with virtually unlimited encoding capacity. This method is also capable of withstanding extreme conditions of plastics manufacturing such as high-temperature casting and lamination. In this context, either a representative population of particles covers a large portion of the packaged surface, or an individual code consisting of a sequence of multiple particles is placed at a well-defined location. Although this method is capable of both techniques, the latter is presented here. Multiple uniquely encoded PUA particles were suspended in a PUA prepolymer mix, laminated onto or embedded within the surface of an object and hardened in place by ultraviolet exposure, a common post-processing step in industrial packaging[33]. A sequence of particles on the surface can be used to uniquely identify the object with an encoding capacity of $(C^S)^N$ for asymmetric particles and $(C^S/2)^N$ for symmetric particles, where N is the number of particles deposited. Randomly embedding 10 particles from a set of just 1,000 unique asymmetric particles yields an encoding capacity of $\sim(1{,}000)^{10}$, or 10^{30}, enough to uniquely barcode every manufactured product on Earth. Application of this technique to anti-counterfeiting of pharmaceutical packaging is illustrated in Fig. 3a (see Methods for surface-encoding protocol). Despite the complex background of the blister pack surface, all decoded spectra fell within 5 sigma of the training centroids (Fig. 3c). Remarkably, PUA-based RGB training data are not required, as shown by successful use of PEGDA-based training data for UCNs 3–5 and 7 (Fig. 2e). PUA particles and the surrounding laminate have identical refractive indices, rendering them invisible unless illuminated with the proper NIR source (Fig. 4 and Supplementary Movie 1). These particles withstand exposure to high-temperature casting up to 260 °C in molten plastics as ubiquitous as poly(ethylene terephthalate) with no impact on decoding, unlocking applications where durable, embedded barcodes are of use (Supplementary Fig. 10). Particles are also insensitive to repetitive illumination and ambient light, a distinct advantage over fluorescently labelled particles that must be stored in the dark[5,17]. A survey of remaining technical risks might lead one to suspect a need for dense particle packing and an accompanying accuracy trade-off due to potential particle overlap. However, the small number of particles required eliminates this challenge. For instance, for the deposition of 10 particles with dimensions of $\sim$250 × 70 μm and a field of view of roughly 10 mm, inter-particle spacing of 300–500 μm at maximum would be needed to provide a comfortable buffer at the edges of the field. In comparison, low-end consumer inkjet printers can reliably space individual dots of ink at 300 dots per inch, or one dot every 80 μm, rendering accurate particle deposition a trivial obstacle to practical success.

Notably, decoding is not limited to microscope-based instrumentation. Figure 4 illustrates image acquisition with a portable apparatus consisting of an Apple iPhone 4S and a ×20 objective. Images are shown in Fig. 4 to demonstrate applicability of this method over a range of complex substrates including pharmaceutical packaging, paper currency, credit cards, curved ceramic objects, reproduced artwork and high-temperature-cast polystyrene. Implementation of quantitative decoding with this portable apparatus would be straightforward, as the central components (CCD detector + magnification) are identical to those of the microscope-based apparatus.

Multiplexed microRNA detection

In addition to enabling new applications, this architecture expands the practical encoding capacity of multiplexed bioassays beyond that of commercial kits by orders of magnitude[1,2]. PEGDA particles with distinct coding and bioassay regions were synthesized, with one set containing a microRNA (miRNA) probe for miR-210 and

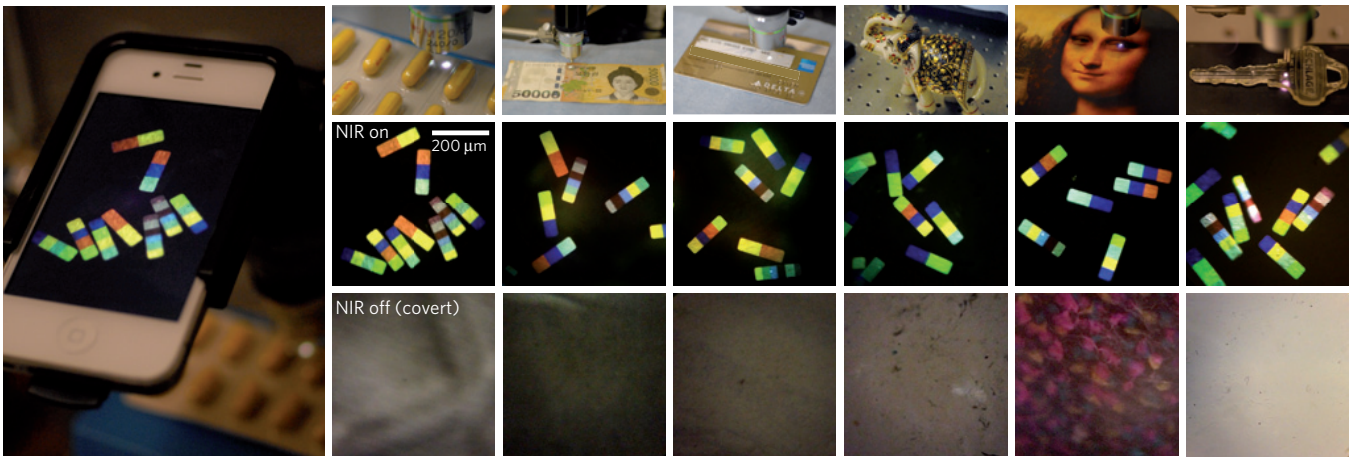

Figure 4 | Imaging of encoded particles with portable decoder in challenging settings. Top: Image acquisition using a portable decoder (Apple iPhone 4S, ×20 objective). Middle and bottom: Acquired image on exposure to 1 W 980 nm laser excitation (middle) and in the absence of NIR excitation (bottom), demonstrating covert operation for (left to right) pharmaceutical blister packs, currency, credit cards, curved ceramic objects, artwork and high-temperature-cast polystyrene objects.

another containing a probe for miR-221 (refs 34,35; Methods for details). The encoding region contains 5 stripes, yielding an encoding capacity of the order of 10^5, and miRNA probes were linked into the bioassay region at particle synthesis using a previously described process[34,35] (Fig. 1e). Mixtures of the 2 sets of particles were added to solutions containing 500 amol of miR-210, miR-221, both miR-210 and 221, or no miRNA, and further processed to read out assay results[34] (Fig. 1f,g). The composite images shown in Fig. 3b and Supplementary Fig. 8 demonstrate successful multiplexed miRNA detection, and that our encoding strategy has negligible impact on the fluorescence intensity observed in the probe region, which is an important criterion for quantifying biomolecule concentrations. RGB code values tightly cluster to the training data centroids for errorless decoding (Fig. 3c). In addition, gadolinium doping of UCNs at 30 mol% yields encoded particles that may be readily manipulated by an externally applied magnetic field (Supplementary Figs 11 and 12 and Movie 2). This is particularly advantageous for applications that require enhanced mass transfer or efficient particle collection.

Outlook

The exceptional performance of our architecture in practical settings represents a significant step towards widespread use in challenging, high-value applications. The mere ability to tune particle material properties without impacting encoding performance unlocks a vast potential for immediate in-line integration of encoded particles into complex manufacturing processes or even consumer products. With modest expansion of the available colour palette or number of stripes per particle, for which no foreseeable impediment exists, single-particle encoding capacities will increase very rapidly. We predict magnetic contact printing or modified inkjet methods giving rise to high-velocity, patterned deposition of multiple particles as a formidable industrial labelling tool. Embedding particles into products at the time of manufacture through three-dimensional printing or liquid casting may also be a powerful anti-counterfeiting technique. This flexible architecture immensely expands the scope of what is possible for encoded particles, promising to accelerate incorporation into a broadening range of modern industrial processes.

Methods

Materials. All chemicals were of analytical grade and used without further purification: $GdCl_3{\bullet}6H_2O$ (Aldrich, 99.9%), $YCl_3{\bullet}6H_2O$ (Aldrich, 99.9%), $YbCl_3{\bullet}6H_2O$ (Aldrich, 99.9%), $TmCl_3{\bullet}6H_2O$ (Aldrich, 99.9%), NH_4F (Aldrich, 99.9%), oleic acid (Aldrich, technical grade, 90%), poly(styrenesulphonate) (Aldrich, M_w~70,000 Da), PEGDA (Aldrich, M_n = 700 Da), 2-hydroxy-2-methylpropiophenone (photo-initiator, Aldrich), PUA (MINS-311RM, Minuta Tech), polystyrene (Aldrich, M_w = 280,000 Da), poly(ethylene terephthalate) (Aldrich #429252), DNA probes and RNA target sequences (IDT).

Synthesis of UCN. UCNs were synthesized as described previously[25]. Three millilitres of NaOH (0.6 g) solution was mixed with 10 ml of ethanol and 10 ml of oleic acid under vigorous stirring. Two millilitres of $RECl_3$ (0.2 M, RE = Y, Yb, Er, Tm, Gd) and 2 ml of NH_4F (2 M) were then added dropwise into the mixture. The solution was transferred to a 50 ml Teflon-lined autoclave and heated at 200 °C for 2 h. The autoclave was allowed to cool naturally to room temperature. Ethanol was used to collect the precipitated products, which were then purified by centrifugation, washed several times with ethanol and deionized water, and finally redispersed in cyclohexane.

Microfluidic device fabrication. Microfluidic devices were fabricated as described previously[3,11]. Briefly, PDMS (Sylgard 184, Dow Corning) was mixed with a curing agent in a 10:1 ratio and degassed under vacuum for 30 min. Degassed PDMS was poured onto an SU-8 master mould and cured overnight at 65 °C. Channels were then cut out of the mould and bonded with a glass slide coated with partially cured PDMS to assure oxygen permeability. The assembled devices were fully cured overnight at 65 °C. The dimensions of the PDMS channel are 300 µm in width and 36 µm in height.

Synthesis of UCN-integrated particles. PUA particles were synthesized using SFL as described previously[3,11]. Briefly, photomasks were designed using AUTOCAD 2011 and printed with a high-resolution printer at CAD Art Services. The mask was placed in the field-stop of the microscope (Zeiss Axio Observer) before synthesis. The UCN-containing monomer solution was composed of 150 mg of UCNs in 300 µl of PUA prepolymer solution (90% (v/v) PUA, 10% (v/v) photo-initiator). The microfluidic channel was loaded with the composite monomer solution, aligned on the microscope stage, and subjected to a pressure-driven flow. In every synthesis cycle, monomer flow was halted (350 ms) and particles were photo-polymerized in the device using ultraviolet light (Lumen 200, Prior Scientific) filtered through a dichroic filter set (11000v3-UV, Chroma Technology, 365 nm, 100 ms exposure time). The polymerized particles were then convected into a collection tube for 500 ms. Synthesis occurred at a rate of ~5 particles s^{-1}. PUA particles were rinsed 8 times with ethanol/PEG200 (1:1 (v/v)) and stored in ethanol.

For PEG hydrogel particles, UCN-containing monomer solution consisting of 45% (v/v) PEGDA (Mn = 700), 40% (v/v) UCNs (0.5 mg μl^{-1}), 10% (v/v) poly(styrenesulphonate) and 5% (v/v) photo-initiator) was loaded into the PDMS microfluidic device and synthesized using SFL as described above. After synthesis, PEG particles were rinsed 3 times with 1× TET (1 × TE with 0.05% (v/v) Tween 20).

Spectral properties of UCN-integrated particles. To ensure spectral consistency of UCN-integrated particles, we examined particle-to-particle variation of RGB pixel values and plotted histograms for 50 particles of each colour (Supplementary

Fig. 2). The average coefficient of variation across all particles and UCN colours was 2%. We fit a Gaussian mixture model to quantify RGB distribution and characterize a specific emission 'colour' for each particle. For each particle cluster, we show 3-, 4- and 5-sigma contour ellipses derived from this analysis. Our RGB scatter plot reveals that cluster overlap occurs only past six standard deviations from the mean, implying an expected error rate of less than 1 ppb.

Surface-encoding protocol. UCN-integrated PUA particles were dispersed in a laminating solution composed of PUA and photo-initiator in a 9:1 (v/v) ratio. Five microlitres of the particle-containing laminating solution was then drop-cast onto the substrate and photo-polymerized for 30 s with a hand-held 365 nm ultraviolet lamp. A 1 W 980 nm NIR laser was used to excite the labelled substrates and luminescence images were taken using either the Apple iPhone 4S or Nikon D200.

Multiplexed miRNA bioassay. The assay was conducted as described previously[34,35]. Reactions were carried out in a final volume of 50 µl inside a 0.65 ml Eppendorf tube. Each reaction contained a total of 75 particles (25 particles of each type: standard miR-221, spectrally encoded miR-221, spectrally encoded miR-210). Target incubations were carried out in miRNA hybridization buffer for 90 min at 55 °C using a thermoshaker (Benchmark, 1,500 r.p.m.). Post-incubation, particles were rinsed with three 500 µl volumes of miRNA rinse buffer (RB) using centrifugation. After each rinse, supernatant was manually aspirated, leaving 50 µl of solution and particles in the reaction tube. Two hundred and thirty-five microlitres of a ligation mastermix that was prepared using 100 µl 10× NEB2 (New England Bio), 900 µl TET, 800 U ml^{-1} T4 DNA ligase (New England Bio), 40 nM biotinylated universal linker sequence (IDT) and 250 nM ATP (New England Bio) was then added to the reaction for a 30 min incubation at 21.5 °C and 1,500 r.p.m. Particles were rinsed three more times using miRNA RB and incubated with streptavidin–phycoerythrin (Life Technologies) at a final concentration of 2 µg ml^{-1} for 45 min at 21.5 °C and 1,500 r.p.m. After three more rinses with miRNA RB, particles were exchanged into PTET (TET with 25% (v/v) PEG-200) for imaging.

Received 26 August 2013; accepted 4 March 2014; published online 13 April 2014

References

1. Cederquist, K., Dean, S. & Keating, C. Encoded anisotropic particles for multiplexed bioanalysis. *WIREs Nanomed. Nanobiotechnol.* **2,** 578–600 (2010).
2. Birtwell, S. & Morgan, H. Microparticle encoding technologies for high-throughput multiplexed suspension assays. *Integrative Biol.* **1,** 345–362 (2009).
3. Pregibon, D., Toner, M. & Doyle, P. Multifunctional encoded particles for high-throughput biomolecule analysis. *Science* **315,** 1393–1396 (2007).
4. Lee, H., Kim, J, Kim, H. & Kwon, S. Colour-barcoded magnetic microparticles for multiplexed bioassays. *Nature Mater.* **9,** 745–749 (2010).
5. Braeckmans, K. *et al.* Encoding microcarriers by spatial selective photobleaching. *Nature Mater.* **2,** 169–173 (2003).
6. Mitrelias, T. *et al.* Enabling suspension-based biochemical assays with digital magnetic microtags. *J. Appl. Phys.* **107,** 09B319 (2010).
7. Dejneka, M. *et al.* Rare earth-doped glass microbarcodes. *Proc. Natl Acad. Sci. USA* **100,** 389–393 (2003).
8. Nicewarner-Pena, S. *et al.* Submicrometer metallic barcodes. *Science* **294,** 137–141 (2001).
9. Kang, E. *et al.* Digitally tunable physicochemical coding of material composition and topography in continuous microfibres. *Nature Mater.* **10,** 877–883 (2011).
10. Lin, C. *et al.* Submicrometre geometrically encoded fluorescent barcodes self-assembled from DNA. *Nature Chem.* **4,** 832–839 (2012).
11. Appleyard, D., Chapin, S., Srinivas, R. & Doyle, P. Bar-coded hydrogel microparticles for protein detection: synthesis, assay and scanning. *Nature Protocols* **6,** 1761–1774 (2011).
12. Cunin, F. *et al.* Biomolecular screening with encoded porous-silicon photonic crystals. *Nature Mater.* **1,** 39–41 (2002).
13. Zhao, Y. *et al.* Multifunctional photonic crystal barcodes from microfluidics. *NPG Asia Mater.* **4,** e25 (2012).
14. Gerver, R. *et al.* Programmable microfluidic synthesis of spectrally encoded microspheres. *Lab on a Chip* **12,** 4716–4723 (2012).
15. Han, M., Gao, X., Su, J. & Nie, S. Quantum-dot-tagged microbeads for multiplexed optical coding of biomolecules. *Nature Biotechnol.* **19,** 631–635 (2001).
16. Zhao, Y. *et al.* Microfluidic generation of multifunctional quantum dot barcode particles. *J. Am. Chem. Soc.* **133,** 8790–8793 (2011).
17. Fulton, R., McDade, R., Smith, P., Kienker, L. & Kettman, J. Advanced multiplexed analysis with the FlowMetrix(TM) system. *Clinical Chem.* **43,** 1749–1756 (1997).
18. Zhang, F. *et al.* Rare-earth upconverting nanobarcodes for multiplexed biological detection. *Small* **7,** 1972–1976 (2011).
19. Mandecki, W. *et al.* Light-powered microtransponders for high multiplex-level analyses of nucleic acids. *Microfabricated Sensors* **815,** 57–69 (2002).
20. Battersby, B. *et al.* Toward larger chemical libraries: Encoding with fluorescent colloids in combinatorial chemistry. *J. Am. Chem. Soc.* **122,** 2138–2139 (2000).
21. Dendukuri, D., Gu, S., Pregibon, D., Hatton, T. & Doyle, P. Stop-flow lithography in a microfluidic device. *Lab on a Chip* **7,** 818–828 (2007).
22. Dendukuri, D., Pregibon, D., Collins, J., Hatton, T. & Doyle, P. Continuous-flow lithography for high-throughput microparticle synthesis. *Nature Mater.* **5,** 365–369 (2006).
23. Bong, K. *et al.* Non-polydimethylsiloxane devices for oxygen-free flow lithography. *Nature Commun.* **3,** 805 (2012).
24. Bong, K. W., Bong, K. T., Pregibon, D. & Doyle, P. Hydrodynamic Focusing Lithography. *Angew. Chem. Int. Ed.* **49,** 87–90 (2010).
25. Wang, F. *et al.* Simultaneous phase and size control of upconversion nanocrystals through lanthanide doping. *Nature* **463,** 1061–1065 (2010).
26. Bogdan, N., Vetrone, F., Ozin, G. & Capobianco, J. Synthesis of ligand-free colloidally stable water dispersible brightly luminescent lanthanide-doped upconverting nanoparticles. *Nano Lett.* **11,** 835–840 (2011).
27. Mahalingam, V., Vetrone, F., Naccache, R., Speghini, A. & Capobianco, J. Colloidal Tm3+/Yb3+-doped $LiYF_4$ nanocrystals: Multiple luminescence spanning the UV to NIR regions via low-energy excitation. *Adv. Mater.* **21,** 4025–4028 (2009).
28. Wang, F. & Liu, X. Upconversion multicolor fine-tuning: Visible to near-infrared emission from lanthanide-doped $NaYF_4$ nanoparticles. *J. Am. Chem. Soc.* **130,** 5642–5643 (2008).
29. Chen, Z. *et al.* Versatile synthesis strategy for carboxylic acid-functionalized upconverting nanophosphors as biological labels. *J. Am. Chem. Soc.* **130,** 3023–3029 (2008).
30. Gorris, H., Ali, R., Saleh, S. & Wolfbeis, O. Tuning the dual emission of photon-upconverting nanoparticles for ratiometric multiplexed encoding. *Adv. Mater.* **23,** 1652–1655 (2011).
31. Choi, N. *et al.* Multiplexed detection of mRNA using porosity-tuned hydrogel microparticles. *Anal. Chem.* **84,** 9370–9378 (2012).
32. Kim, J., Park, K., Kim, Z., Baek, K. & Do, L. Fabrication of low-cost submicron patterned polymeric replica mold with high elastic modulus over a large area. *Soft Matter* **8,** 1184–1189 (2012).
33. Davidson, M. *Pharmaceutical Anti-Counterfeiting: Combating the Real Danger from Fake Drugs* (Wiley, 2011).
34. Chapin, S., Appleyard, D., Pregibon, D. & Doyle, P. Rapid microRNA profiling on encoded gel microparticles. *Angew. Chem. Int. Ed.* **50,** 2289–2293 (2011).
35. Chapin, S. & Doyle, P. Ultrasensitive multiplexed microRNA quantification on encoded gel microparticles using rolling circle amplification. *Anal. Chem.* **83,** 7179–7185 (2011).

Acknowledgements

We thank J. Capobianco for thoughtful guidance and M. Garcia Fierro for critical reading and perspective on the manuscript. The MIT Lincoln Laboratory portion of this work was sponsored by the Department of the Air Force under Air Force Contract number FA8721-05-C-0002. The MIT Campus portion of this work was sponsored by the Office of the Assistant Secretary of Defense for Research and Engineering, the Institute for Collaborative Biotechnologies through grant W911NF-09-0001 from the US Army Research Office, and the Singapore–MIT Alliance and National Science Foundation grants CMMI-1120724 and DMR-1006147. R.L.S. was supported by an NIH T32 GM08334 interdepartmental biotechnology training grant. The work was also supported by the Institute for Collaborative Biotechnologies through grant W911NF-09-0001 from the US Army Research Office. The content of the information does not necessarily reflect the position or the policy of the Government, and no official endorsement should be inferred.

Author contributions

J.L. and P.W.B. contributed equally to this work. J.L. designed the research, conducted most of the experiments, conducted design and synthesis of UCNs, interpreted data and wrote the manuscript. P.W.B. conceived the project, designed experiments, interpreted data, conducted design and synthesis of UCNs, and wrote the manuscript. R.L.S. designed and conducted bioassay experiments. J.J.K. participated in design and synthesis of UCNs. P.S.D. and A.J.S. conceived the project, discussed the results, supervised the study and interpreted data. All authors reviewed and approved the manuscript.

Additional information

Supplementary information is available in the online version of the paper. Reprints and permissions information is available online at www.nature.com/reprints. Correspondence and requests for materials should be addressed to P.S.D

Competing financial interests

The authors declare Provisional US patent applications 61/801, 351 and 61/800, 995, filed 15 March 2013.